Near 5-GHz Longitudinal Leaky Surface Acoustic Wave Devices on $LiNbO_3$/SiC Substrates

Pengcheng Zheng, *Graduate Student Member, IEEE*, Shibin Zhang, *Member, IEEE*, Jinbo Wu, *Graduate Student Member, IEEE*, Liping Zhang, *Graduate Student Member, IEEE*, Hulin Yao, *Graduate Student Member, IEEE*, Xiaoli Fang, *Graduate Student Member, IEEE*, Yang Chen, Kai Huang, and Xin Ou, *Senior Member, IEEE*

***Abstract*— This work demonstrates a group of longitudinal leaky surface acoustic wave (LL-SAW) resonators and filters using thin-film X-cut lithium niobate on silicon carbide ($LiNbO_3$/SiC). An improved design that exploits a nonstandard reflector (NSR) structure to suppress the lateral overtone spurious mode in the LL-SAW response is demonstrated. The fabricated resonators show scalable resonant frequencies from 3.75 to 4.95 GHz, admittance ratios (ARs) between 56.0 and 64.1 dB, and large k_t^2 between 18.3% and 20%. The fabricated filter with a center frequency of 4.84 GHz shows a minimum insertion loss (IL) of 0.88 dB, an out-of-band rejection of 26 dB, and a 3-dB bandwidth (BW) of 457 MHz, partially covering the fifth-generation (5G) N79 band. The filter design tradeoff between SH mode suppression and BW is also demonstrated. The results herein show the great potential of LL-SAW technologies using $LiNbO_3$/SiC substrate for commercial applications in 5G new radio (NR) and Wi-Fi 5/6 bands.**

***Index Terms*— Fifth-generation (5G) N79 band, filters, lithium niobate on silicon carbide ($LiNbO_3$/SiC), longitudinal leaky surface acoustic wave (LL-SAW), resonators, spurious mode suppression.**

Manuscript received 4 May 2023; revised 10 July 2023; accepted 30 July 2023. This work was supported in part by the National Key Research and Development Program of China under Grant 2020YFB2008802; in part by the National Natural Science Foundation of China under Grant 62293520, Grant 62293524, Grant 62204252, and Grant 62231023; in part by the Young Elite Scientists Sponsorship Program by the China Association for Science and Technology (CAST) under Grant 2022QNRC001; and in part by the Shanghai Rising-Star Program under Grant 23QB1405300. *(Pengcheng Zheng and Shibin Zhang contributed equally to this work.) (Corresponding authors: Shibin Zhang; Xin Ou.)*

Pengcheng Zheng, Jinbo Wu, Liping Zhang, Hulin Yao, Xiaoli Fang, Yang Chen, and Xin Ou are with the State Key Laboratory of Functional Materials for Informatics, Shanghai Institute of Microsystem and Information Technology, Chinese Academy of Sciences, Shanghai 200050, China, and also with the Center of Materials Science and Optoelectronics Engineering, University of Chinese Academy of Sciences, Beijing 100049, China (e-mail: ouxin@mail.sim.ac.cn).

Shibin Zhang is with the State Key Laboratory of Functional Materials for Informatics, Shanghai Institute of Microsystem and Information Technology, Chinese Academy of Sciences, Shanghai 200050, China, and also with XOI Technology Company Ltd., Shanghai 201899, China (e-mail: sbzhang@mail.sim.ac.cn).

Kai Huang is with the State Key Laboratory of Functional Materials for Informatics, Shanghai Institute of Microsystem and Information Technology, Chinese Academy of Sciences, Shanghai 200050, China, and also with Shanghai Novel Si Integrated Technology Company Ltd., Shanghai 201815, China.

Color versions of one or more figures in this article are available at https://doi.org/10.1109/TMTT.2023.3305078.

Digital Object Identifier 10.1109/TMTT.2023.3305078

I. Introduction

In THE past decade, significant effort has been devoted to developing low-loss filters with larger bandwidths (BWs) and higher frequencies in response to the technical requirements of radio frequency (RF) front-end wireless communication systems [1], [2]. The incumbent filter technologies dominating the market are mainly based on either surface acoustic wave (SAW) or bulk acoustic wave (BAW) [3], [4], [5], [6], [7]. Nevertheless, the allocated fifth-generation (5G) new radio (NR) and Wi-Fi 5/6 bands can end up demanding a fractional BW as large as 24% above 3 GHz, greatly challenging the capabilities of acoustic filters [8], [9].

The AlN-based BAW devices have been demonstrated to scale the frequency up to 8 GHz [10], due to the thickness-defined frequency. However, the relative BW is limited by the moderate piezoelectric constant e_{33} of AlN [11]. As a comparison, the $LiNbO_3$-based SAW devices inherently have the capability to achieve a wider BW [12]. The major bottleneck of SAW devices is the operating frequency, which is defined by $f_r = v/\lambda$, where v is the phase velocity of the intended acoustic mode and λ is the wavelength. For conventional SAW devices, the velocity of the generally utilized SH-SAW mode is around 3500 m/s [13], [14], [15], indicating that f_r cannot exceed 3.5 GHz using the KrF lithography (248 nm) system. Further reducing the width/height of interdigital transducers (IDTs) electrodes is not a suitable method for mass production, which induces higher losses and degraded power handling. Longitudinal leaky SAW (LL-SAW) mode is a competitive candidate to fulfill the requirement of 5G NR bands, which features about 1.7 times higher velocity (~6000 m/s) than that of SH-SAW mode and large electromechanical coupling coefficient k_t^2 [16], [17], [18]. However, it is well known that SH-SAW resonators as well as LL-SAW resonators based on bulk $LiNbO_3$ or $LiTaO_3$ show low quality factor (Q) due to severe bulk wave radiation [19], [20]. Makkonen et al. [21] demonstrated a 2.8-GHz LL-SAW filter on Y-cut $LiNbO_3$, showing a high velocity of ~6100 m/s, but a large minimum insertion loss (IL) of 2.3 dB and a rounded shape of the passband.

In recent years, SAW devices based on heterogeneous substrates have emerged as a promising technology and have been commercialized (e.g., I.H.P. SAW [22], [23]). Through

bonding $LiNbO_3$ or $LiTaO_3$ thin films on a high-velocity substrate, resonators with boosted Q and k_t^2 can be obtained due to the acoustic waveguide effect [24], [25], [26], [27]. Up to now, the aforementioned high-performance SAW devices mainly focus on the SH-SAW mode, while the LL-SAW devices are still rarely reported, which is due to the insufficient bulk wave velocities of common substrate materials (e.g., Si, quartz, and sapphire). While using a Bragg mirror as a supporting substrate is an alternative [27], [28], [29], the device design and fabrication process would become very complicated. Therefore, the key to achieve high-performance LL-SAW devices is to apply an extremely high-velocity supporting substrate, such as SiC and diamond.

To explore the potential of the SAW technology beyond 4 GHz, this work designs and demonstrates high-performance LL-SAW devices on the thin-film X-cut lithium niobate on silicon carbide ($LiNbO_3$/SiC) substrate. The LL-SAW resonators with optimized designs show high resonant frequency from 3.75 to 4.95 GHz, large admittance ratios (ARs), and large k_t^2. A group of N79 band filters is demonstrated, showing flat passband, excellent BW, low IL, and good out-of-band rejection.

The rest of this article is organized as follows. Section II presents the design of LL-SAW resonators on the X-cut $LiNbO_3$/SiC platform. Section III presents the measured results of the high-performance LL-SAW resonators and filters. Finally, the conclusion is stated in Section IV.

II. Device Design

In this section, the layered LL-SAW configurations are analyzed by using the finite element method (FEM). The critical dimensions of the piezo-layer and electrodes are optimized to achieve the resonator response with large k_t^2, low loss, and weak spurious modes simultaneously.

A. Basic Configurations of LL-SAW Resonators

First, we analyze the acoustic propagation characteristics of the piezoelectric thin film without considering the supporting substrates. The LL-SAW and SH-SAW correspond to the S0 mode and SH0 mode in the piezoelectric thin plate, respectively, which are distinguished according to their dominant displacement components. Using the eigenmode FEM analysis, the piezoelectric coupling factor K^2 of SH0 and S0 with different in-plane orientations (θ) in the X-cut $LiNbO_3$ thin plate is plotted in Fig. 1(a), which is calculated as [30], [31]

$$K^2 = \left(v_o^2 - v_m^2\right)/v_m^2 \tag{1}$$

where v_o and v_m are the simulated velocities under the electrically open and short conditions, respectively. Here, the Euler angle in simulation is $(-\theta, 90°, 90°)$, and the normalized $LiNbO_3$ thickness is 0.25. The mode shapes are also included in the inset. When θ is approximately 32°, the S0 mode shows a K^2 larger than 30%, while the excitation of the SH0 mode is weak. v_m in the material yz plane is plotted in Fig. 1(b). The velocity of the S0 mode is approximately 1.7 times higher than that of the SH0 mode, corresponding to 1.7 times the

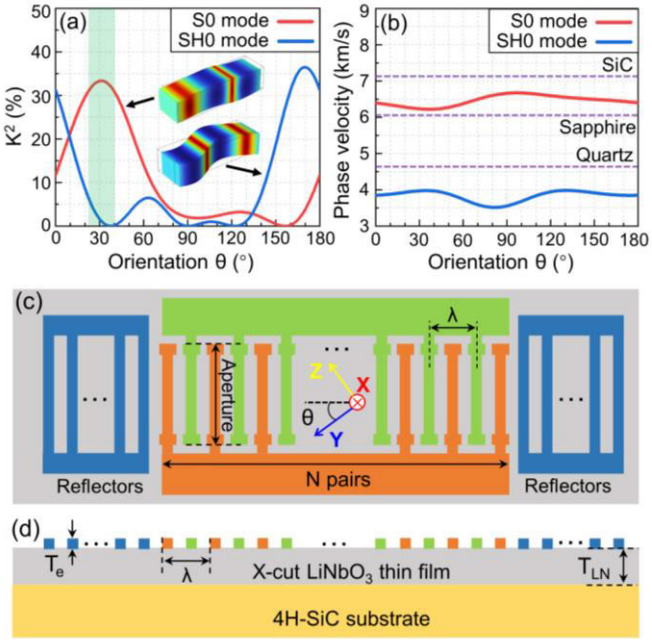

Fig. 1. Simulated (a) K^2 and (b) phase velocities of SH0 and S0 modes in the yz plane of X-cut $LiNbO_3$ thin plate. Schematic of an LL-SAW resonator in the thin-film X-cut $LiNbO_3$/SiC substrate. (c) Top view. (d) Side view.

operating frequency of the SH0 mode under the same feature size. The velocities of the shear bulk wave (SBW) in three supporting substrates (i.e., SiC, sapphire, and Z-quartz) are also plotted (dashed lines) [32], [33], [34], [35], which are higher than that of SH0 mode. When $LiNbO_3$ thin film is bonded onto the abovementioned substrates to excite the SH-SAW mode, a perfect acoustic waveguide in the piezo layer can be obtained. Therefore, the bulk wave radiation is almost suppressed due to the decoupling of the SH component and the shear vertical (SV) component, leading to a significant Q increase of the SH-SAW resonators [36], [37], [38]. In the case of S0 mode, only SiC exhibits sufficiently high velocity to confine the acoustic energy of LL-SAW in the layered substrate. Although diamond possesses a much higher shear wave velocity (v_s = 12 823 m/s) than SiC, it suffers from the high cost and small wafer size, limiting its industrial application in the near future.

The schematic of a one-port LL-SAW resonator is shown in Fig. 1(c) and (d). The resonator consists of IDTs on top of the X-cut $LiNbO_3$ thin film, solidly mounted on the high-velocity 4H-SiC substrate. Two grating reflectors are placed at both lateral ends of the IDTs. The wavelength λ is equal to twice the IDT pitch here. The resonators are oriented at 40° to $+y$-axis (θ = 40°) to maximize k_t^2 of the LL-SAW mode.

First, the FEM SAW simulation is conducted using periodic 2-D models to visualize the acoustic loss of the LL-SAW resonator. λ is set to be 1.6 μm, and h_{Al} is set to be 100 nm. The material loss is neglected in the simulation. The simulated frequency responses of three SAW structures are presented in Fig. 2. The corresponding mode shapes at the resonant frequencies of the LL-SAW modes are also illustrated at the right. The conductance is the real part of the admittance,

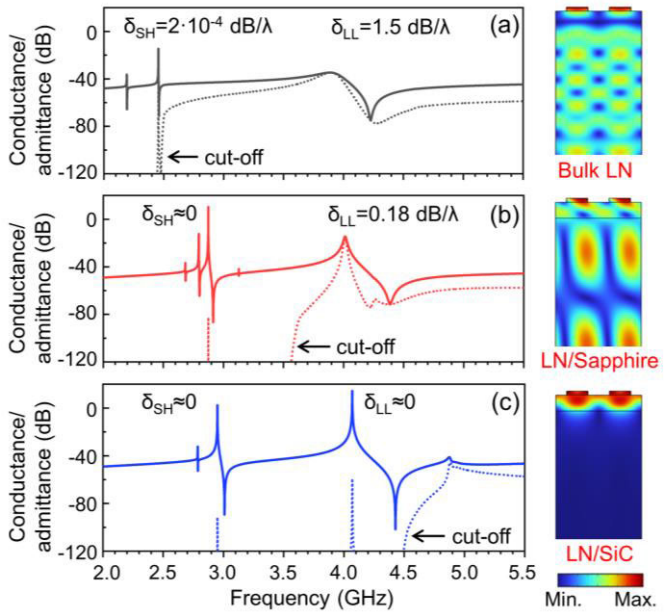

Fig. 2. Simulated admittance and conductance curves of SAW resonators for infinite periodic IDT on (a) bulk X–$Y40°$ $LiNbO_3$, (b) 400-nm X–$Y40°$ $LiNbO_3$/sapphire, and (c) 400-nm X–$Y40°$ $LiNbO_3$/SiC. At the right, the corresponding mode shapes at the resonant frequencies of the LL-SAW modes are illustrated.

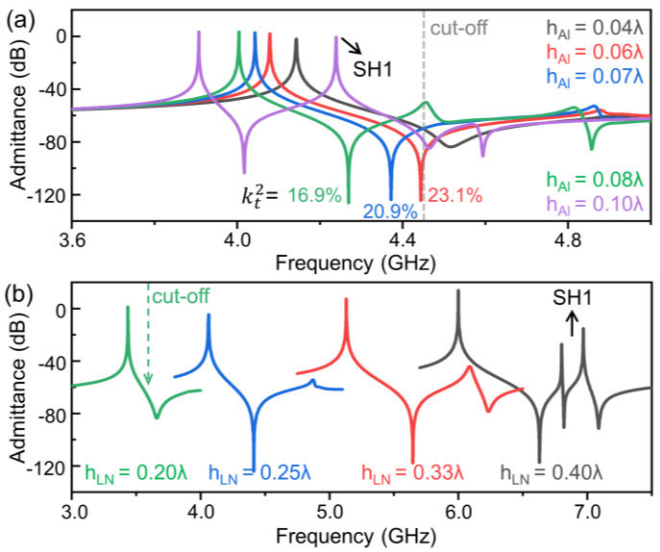

Fig. 3. Simulated admittance curves of LL-SAW resonators for infinite periodic IDT on X–$Y40°$ $LiNbO_3$/SiC with different (a) IDT thicknesses and (b) wavelengths λ (or h_{LN}/λ).

and its magnitude indicates the acoustic loss caused by the bulk wave radiation. The frequency where the conductance suddenly drops from a finite value to zero is called the cutoff frequency [39], [40]. The cutoff frequency is approximately calculated as the ratio of the shear bulk wave velocity in the substrate to λ.

In the case of conventional SAW on bulk $LiNbO_3$ substrate [in Fig. 2(a)], the cutoff frequency is located near the response of the SH-SAW mode, which is much lower than that of the LL-SAW mode. Therefore, the SH-SAW exhibits a low attenuation of 2×10^{-4} dB/λ, while the LL-SAW shows a high attenuation of 1.5 dB/λ. For the case of layered SAW on $LiNbO_3$/sapphire substrate [in Fig. 2(b)], the cutoff frequency as well as the resonant frequency of both modes significantly increase, and the lossless SH-SAW response is obtained. Nevertheless, the attenuation of the LL-SAW mode is still large ($\delta_{LL} = 0.18$ dB/λ) due to the insufficient velocity of the sapphire. When the supporting substrate is replaced by SiC with a higher bulk wave velocity, the cutoff frequency increases to 4.5 GHz, as shown in Fig. 2(c). This is above the antiresonance of the LL-SAW. In addition, bulk wave radiation patterns can be hardly seen in the mode shape, indicating the negligible acoustic leakage for the LL-SAW resonator based on $LiNbO_3$/SiC substrate.

B. Optimization of Resonator Structure

The relationship between the IDT size and the $LiNbO_3$ layer thickness has also been optimized. First, the LL-SAW resonators with different normalized aluminum thicknesses (h_{Al}/λ) are simulated using periodic 2-D models [in Fig. 3(a)]. The thickness of the $LiNbO_3$ layer is set to be 400 nm, and λ is set to be 1.6 μm. The cutoff frequency is also marked. In the case of $h_{Al} = 0.04\lambda$, despite the sharp resonance, the antiresonance is above the cutoff frequency due to the relatively slight mass loading, resulting in low Q at the antiresonance. When h_{Al} increases from 0.06λ to 0.08λ, the antiresonances shift below the cutoff frequency and show sharp responses, and k_t^2 of the LL-SAW resonators decrease from 23.1% to 16.9%. Besides, the spurious SH1 mode is observed at the high-frequency side of LL-SAW mode if IDT is relatively thick. In short, the normalized thickness of aluminum between 0.06 and 0.08 is preferred when designing an LL-SAW resonator on $LiNbO_3$/SiC.

Next, the LL-SAW resonators with a fixed h_{Al} of 0.065 but different λ (or normalized $LiNbO_3$ thickness, h_{LN}/λ) are simulated, as shown in Fig. 3(b). Due to the velocity dispersion characteristic of the LL-SAW mode, the relative cutoff frequencies vary with h_{LN}/λ. The resonator with $h_{LN}/\lambda = 0.40$ suffers from the strong SH1 spurious response, while the resonator with $h_{LN}/\lambda = 0.20$ shows low Q at the antiresonance. Thus, the normalized $LiNbO_3$ thickness needs to be between 0.25 and 0.33.

C. Spurious Mode Suppression

Following the above guideline, an LL-SAW resonator with 90 pairs of IDTs and ten pairs of reflectors on 400-nm X–$Y40°$ $LiNbO_3$/SiC is simulated using 2-D FEM in Fig. 4(a). The mechanical loss is assumed to be 1/2000. h_{LN}/λ is set to be 0.267, and h_{Al}/λ is set to be 0.067. Although the AR of the LL-SAW is larger than 80 dB, there is a strong spurious mode located between the resonance and the antiresonance, leading to severe passband ripples in the filter response. The stress distributions of the simulated LL-SAW at the resonance, 4517 MHz, and at the antiresonance are presented in Fig. 4(b)–(d). At the resonant frequency, the acoustic energy is well confined in the $LiNbO_3$ layer, and the bulk wave radiation in the substrate cannot be observed. In contrast, since

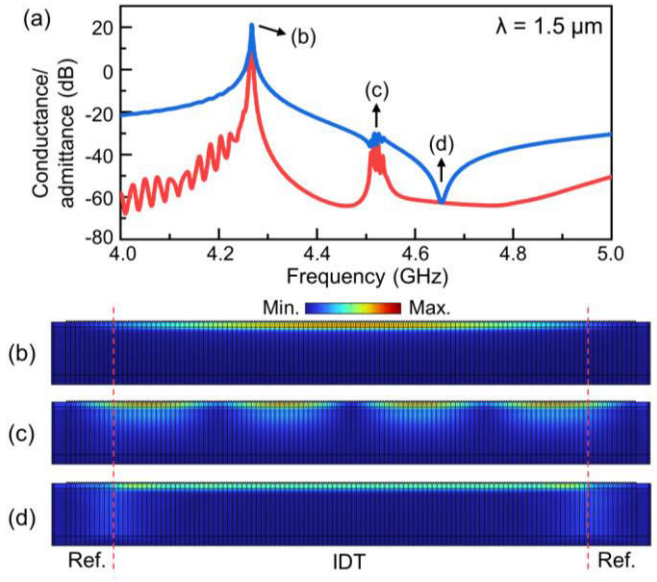

Fig. 4. (a) Simulated admittance and conductance responses of an LL-SAW resonator with 90 IDT pairs. The stress distributions of the LL-SAW resonator at (b) resonant frequency, (c) 4517 MHz, and (d) antiresonant frequency.

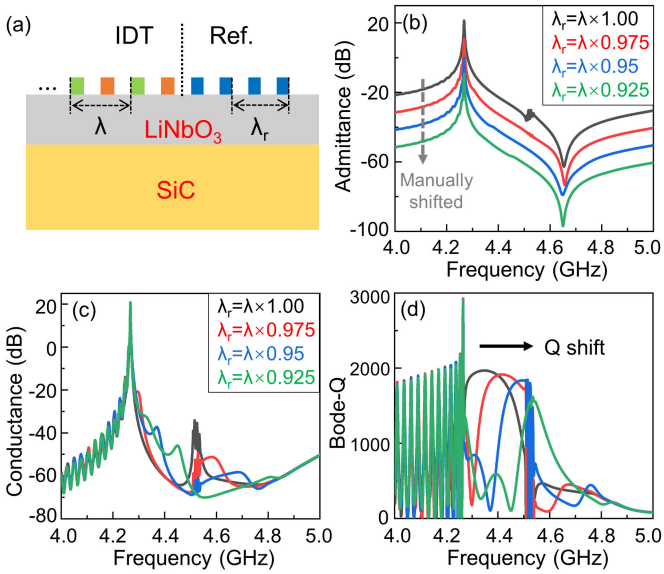

Fig. 5. (a) Side view of the NSR configuration. The simulated responses of LL-SAW resonators with different normalized λ_r. (b) Admittance, (c) conductance, and (d) Bode-Q.

the antiresonant frequency is close to the cutoff frequency, acoustic energy leaks partially into the substrate at both ends of the IDT, leading to moderate Q at the antiresonance. In Fig. 4(c), it can be noticed that the spurious mode is a high-order overtone response formed in the vicinity of the surface with metalized grating. The lateral overtone mode is also generated at the high-frequency side of antiresonance in the SH-SAW resonator [41], but it does not affect the passband of the SH-SAW filter.

In order to suppress the generation of the lateral overtone mode, the potential idea is to break the periodicity of the

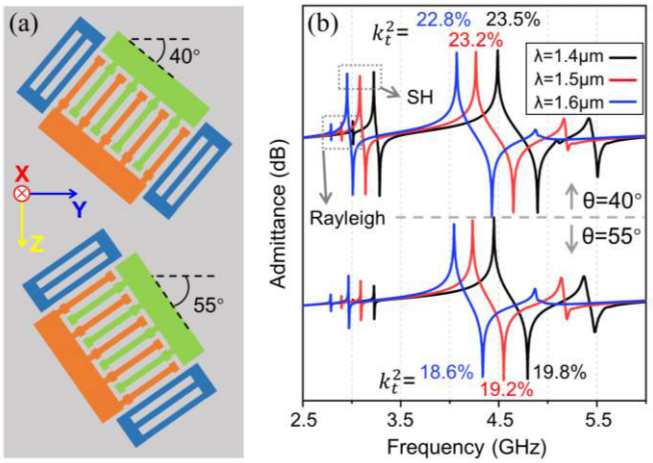

Fig. 6. (a) Schematic of SH-SAW suppression through orientation modulation. (b) Simulated admittance curves of LL-SAW resonators with infinite periodic IDT oriented at 40° and 55°.

metalized grating on the surface. As shown in Fig. 5(a), a novel configuration, the period of reflectors (λ_r) is lower than λ, is proposed, which is called nonstandard reflector (NSR). The 90-pair LL-SAW resonators with a fixed λ of 1.5 μm but different λ_r are simulated. As shown in Fig. 5(b), the in-band spurious mode is successfully suppressed while keeping the resonant and antiresonant frequencies unchanged when the NSR configuration is employed. The conductance curves of the simulated resonators are plotted in Fig. 5(c). Compared to the resonator with standard reflector (SR) configuration ($\lambda_r = \lambda$), the conductance of the resonators with NSR is higher at some frequency ranges, indicating more acoustic leakage. The Bode-Q curves are also plotted in Fig. 5(d). For the conventional case, a wide high-Q frequency window lower than the antiresonant frequency can be obtained. However, when λ_r decreases, the Bode-Q curve shifts to a higher frequency, and the high-Q frequency window becomes narrower. In brief, the lateral overtone mode has been effectively suppressed at the expense of the Q of resonators.

In addition to the in-band spurious mode, the out-of-band spurious mode, especially at the lower frequency band, needs to be mitigated for the coexistence with 4G LTE bands. As analyzed in Section II-A, both LL-SAW and SH-SAW modes are excited in X-cut $LiNbO_3$, and an optimum in-plane orientation can be obtained that k_t^2 of SH-SAW is minimized, whereas k_t^2 of LL-SAW keeps large. According to the top-view diagram in Fig. 6(a), the resonators oriented to Y-40° and Y-55° with different λ values are simulated using the periodic model and shown in Fig. 6(b). When θ is 40°, k_t^2 of LL-SAW modes reaches the maximum, but the SH-SAW responses with high magnitudes are also generated. When θ is 55°, the SH-SAW modes are significantly mitigated at the expense of approximately a 4% reduction in k_t^2 of the LL-SAW modes.

To sum up, in Section II, high-frequency spurious-free LL-SAW resonators with large k_t^2 and high Q are designed using X-cut $LiNbO_3$/SiC. The optimized LL-SAW devices will be experimentally demonstrated in Section III.

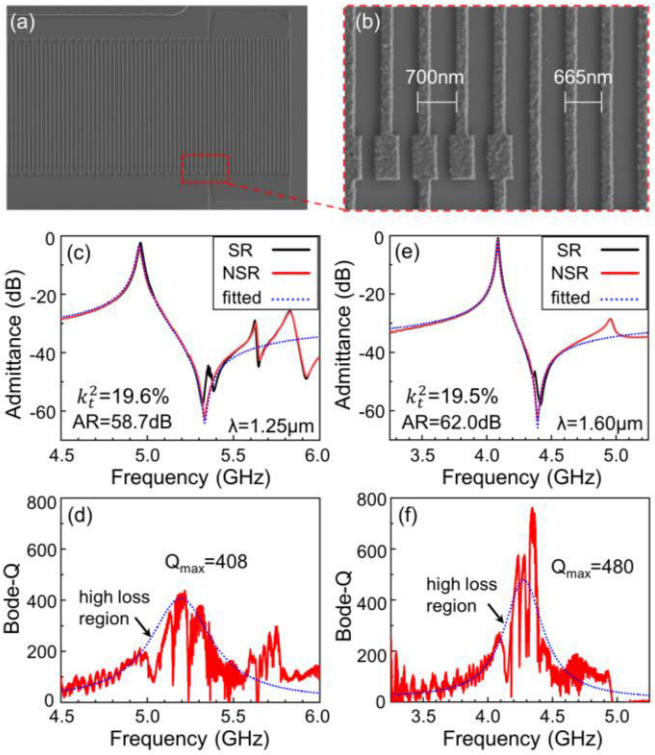

Fig. 7. (a) and (b) SEM images of a fabricated LL-SAW resonator with NSR configuration and λ of 1.4 μm. Measured and fit (c) admittance and (d) Bode-Q of resonators with λ of 1.25 μm. Measured and fit (e) admittance and (f) Bode-Q of resonators with λ of 1.60 μm.

III. Experimental Results and Discussion

A. Fabrication Process and Measurements

A 4-in single-crystal $LiNbO_3$/SiC heterogeneous substrate was fabricated using the ion-slicing technology [42], [43]. First, helium ions (He^+) were implanted into an X-cut $LiNbO_3$ wafer to form a damaged layer below the surface of the wafer. Subsequently, the implanted wafer was directly bonded to the high-resistance 4H-SiC wafer. Then, the $LiNbO_3$ thin film was split from the bulk wafer and transferred onto the SiC wafer through the postannealing process. Finally, the thin-film $LiNbO_3$/SiC was thinned to 410 nm using the chemical-mechanical polishing (CMP) process.

The devices were in-house fabricated. The device patterns were prepared by electron-beam lithography (EBL), electron-beam evaporation (EBE), and liftoff process. The thickness of IDT electrodes is 100 nm, consisting of 5-nm Ti and 95-nm Al. The fabricated devices were characterized by a Keysight E5071C vector network analyzer with a 50-Ω characteristic impedance at room temperature in air.

B. LL-SAW Resonators

To validate the effectiveness of the NSR structure, the LL-SAW resonators with $\lambda_r = \lambda$ and $\lambda_r = 0.95\lambda$ are measured and compared. Fig. 7(a) and (b) shows the scanning electron microscope images of an LL-SAW resonator with λ of 1.4 μm. The pitch of IDTs is about 700 nm, while the pitch of reflectors is about 665 nm (700 × 0.95 nm). The piston electrode structure is adopted to suppress the transverse modes,

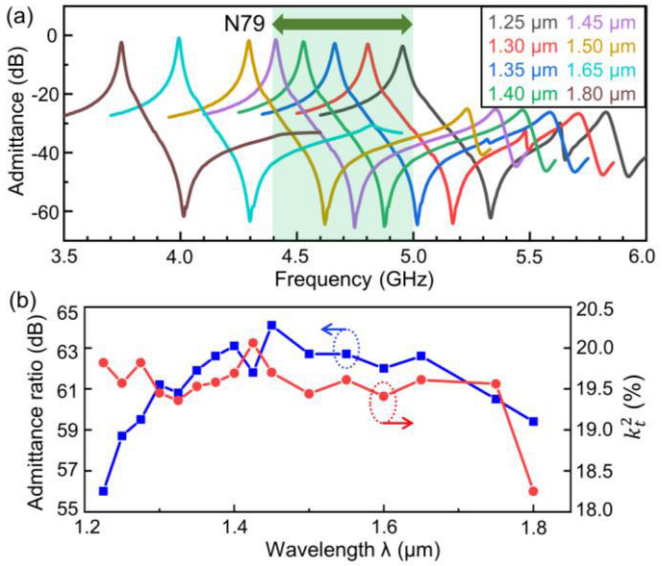

Fig. 8. (a) Measured admittance curves of the fabricated LL-SAW resonators with different λ's. (b) Extracted AR and k_t^2 of the resonators with different λ's.

and thus, the metallization of the IDTs and reflectors is set to be 30% to improve the effect of piston mode operation [44].

The measured and fit admittance responses of the resonators with λ of 1.25 and 1.60 μm are shown in Fig. 7(c) and (e), respectively. The corresponding Bode-Q curves are shown in Fig. 7(d) and (f). The resonators with conventional SR configuration (black solid lines) exhibit strong spurious modes near the antiresonances, consistent with the simulated results shown in Fig. 4. By using the proposed NSR structure, the lateral overtone modes are successfully suppressed and sharp antiresonances are obtained.

The resonator with λ of 1.25 μm shows a high f_r of 4.95 GHz, a large k_t^2 of 19.6%, and a fit Bode-$Q_{\max}$ of 408. The resonator with λ of 1.60 μm shows f_r of 4.08 GHz, a large k_t^2 of 19.5%, and a fit Bode-$Q_{\max}$ of 480. As seen from Fig. 7(d) and (f), despite the high Q of both LL-SAW resonators, there are obvious Q degradation regions at the high-frequency side of the resonances, which are also consistent with the previously simulated results.

Fig. 8(a) presents the admittance curves of LL-SAW resonators orientated at 40° with different λ, showing the high f_r from 3.75 to 4.95 GHz, as well as the high phase velocities from 6.19 to 6.75 km/s. Similarly, the NSR configuration with $\lambda_r = 0.95\lambda$ is used to achieve the in-band spurious-free responses. It is expected that the LL-SAW resonators are enabled to exceed 6 GHz by using KrF lithography. The AR and k_t^2 are extracted in Fig. 8(b). When λ is smaller than 1.8 μm, the LL-SAW resonators exhibit a high average k_t^2 of 19.6%. This is already larger than that of highly doped AlScN BAW resonators reported in [45] and [46]. As λ increases, the AR first increases, reaches the maximum of 64.1 dB, and then decreases. The upward trend may be related to the reduced ohmic loss (i.e., R_s in the mBVD model [47]). However, as analyzed in Section II-B, larger λ corresponds to smaller normalized $LiNbO_3$ thickness, leading to higher attenuation at the antiresonance and decreased AR of resonators.

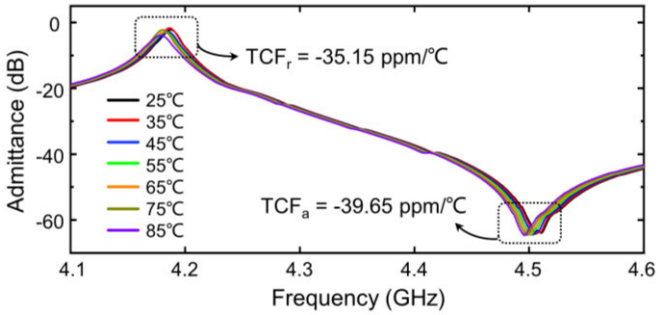

Fig. 9. Measured admittances of the resonators with λ of 1.55 μm under different working temperatures.

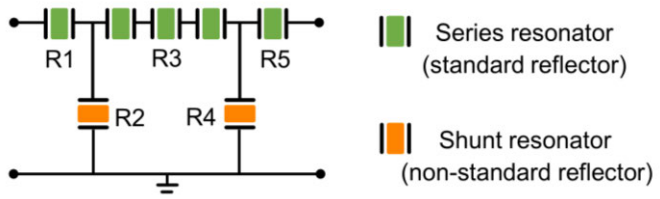

Fig. 10. Topology of five-order ladder-type filters.

The temperature stability of the LL-SAW resonator is also investigated. The resonator with λ of 1.55 μm is tested in the temperature range of 25 °C–85 °C, and the measured results are shown in Fig. 9. The fit first-order temperature coefficients of frequency (TCFs) at the resonance and antiresonance are −35.15 ppm/°C and −39.65 ppm/°C, respectively. Through adding a SiO_2 layer with the positive TCF between $LiNbO_3$ thin film and SiC, the TCF of LL-SAW devices can be further improved.

C. Ladder-Type Filters for N79 Band

Based on the measured results of LL-SAW resonators, we attempt to design LL-SAW filters toward the 5G N79 band (4400–5000 MHz) application. The physical BW of the N79 band is about 1.7 times the measured resonance-to-antiresonance distance (∼350 MHz) of the LL-SAW resonators. Thus, it is difficult to achieve high out-of-band rejection while covering the full band for ladder-type filters due to the design tradeoff between BW and out-of-band rejection [48].

Filter-A and filter-B with the order of five are designed to cover the partial N79 band, and their topology is shown in Fig. 10 without external matching elements. The second resonator in the series branch is split into three cascaded resonators to improve power durability. The design parameters of resonators in the filters are calculated under the guideline introduced in [49] and [50] and listed in Table I.

Filter-A is oriented to Y-40° in the yz plane to maximize the BW. The wafer-probe measured responses of fabricated filter-A and the corresponding resonators are shown in Fig. 11(a). Filter-A shows a high f_c of 4.84 GHz, a 3-dB BW of 457 MHz, and a low minimum IL of 0.88 dB. To suppress the SH-SAW mode while maintaining a large BW, filter-B is oriented to Y-55°. Fig. 11(b) presents the measured results

TABLE I
KEY DESIGN PARAMETERS OF RESONATORS IN FILTERS

	R1	R2	R3	R4	R5
Filter-A					
Piezo-layer	410 nm X-Y40° $LiNbO_3$				
λ (μm)	1.292	1.432	1.274	1.432	1.292
N_{IDT}	90	111	90	111	90
Aperture ($\times\lambda$)	14	19	14.3	19	14
Filter-B					
Piezo-layer	410 nm X-Y55° $LiNbO_3$				
λ (μm)	1.275	1.398	1.264	1.398	1.275
N_{IDT}	92	117	90	117	92
Aperture ($\times\lambda$)	15	20	16	20	15

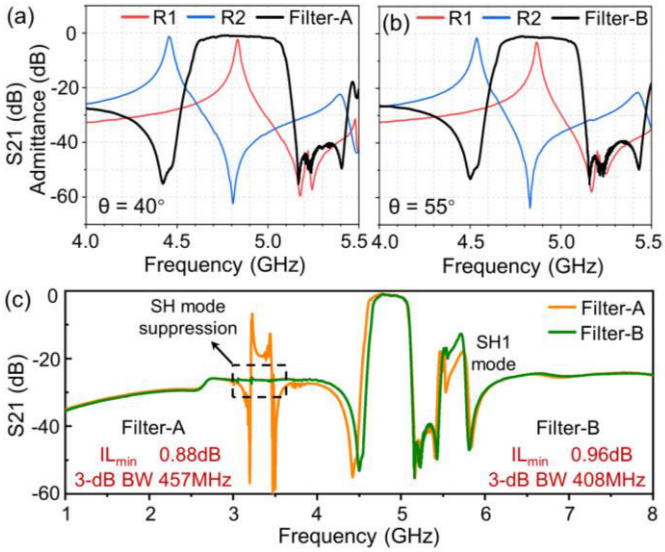

Fig. 11. Measured responses of (a) filter-A and (b) filter-B. (c) Comparison of $S21$ responses of filter-A and filter-B over a wide frequency range.

of the filter-B, showing a high f_c of 4.88 GHz, a 3-dB BW of 408 MHz, and a low minimum IL of 0.96 dB. Since the overtone mode is located near the antiresonance of the resonator, the series resonators with higher frequencies in the ladder-type filters adopt SR configuration rather than NSR configuration to decrease the IL in the upper passband. The $S21$ responses of filter-A and filter-B are compared over a wide frequency range in Fig. 11(c). Both filters show the same upper cutoff frequency, close out-of-band rejection (∼26 dB), and sharp roll-off. Although filter-B has a narrower passband than filter-A, it exhibits spurious-free lower stopband response, indicating the design tradeoff of LL-SAW filters.

D. Discussion

Finally, the comparison of the filter in this work with the reported state-of-the-art acoustic-only filters is summarized in Table II. The fabricated LL-SAW filter exhibits comprehensive performance comparable to AlN-based BAW [7], [53] and $LiNbO_3$-based Lamb wave [51], [52] filters. Besides, the LL-SAW technology has more simplified manufacturing process and lower cost, and it would become a competitive solution for 5G NR bands. Although the SH-SAW technology based on heterogeneous substrates [12], [25] naturally has the

TABLE II
COMPARISONS OF HIGH-FREQUENCY ACOUSTIC-ONLY FILTERS

Ref.	platform	f_r (GHz)	IL_{min} (dB)	3-dB BW (MHz)	OoB (dB)
[51]	A1 suspended $LiNbO_3$	4.5	1.7	450	13
[52]	A1 suspended $LiNbO_3$	4.75	1.0	600	30
[7]	SMR-BAW AlScN	5.25	1.0	~230	40
[53]	FBAR AlScN	5.66	1.79	452	40
[21]	LL-SAW bulk $LiNbO_3$	2.8	2.3	132.5	15
[54]	LL-SAW $LiNbO_3$/SiC	6.12	2.36	483	10
[12]	SH-SAW $LiNbO_3$/Ox/Si	3.67	0.73	1080	9
[25]	SH-SAW $LiNbO_3$/SiC	2.62	1.06	330	17.7
This work	**LL-SAW $LiNbO_3$/SiC**	**4.84**	**0.88**	**457**	**26**

advantages of wideband capability and low IL, the operating frequency is its major bottleneck. Compared to the LL-SAW filter in our previous work [54], the filter in this work exhibits a more balanced RF performance. Such progress is primarily due to the improvements in the material quality of transferred $LiNbO_3$ thin film and electrode layer. In addition, the structural parameters of the resonator (in Section II) and the topology of the filter are also optimized.

The Q and TCF of the demonstrated resonators are moderate, and the magnitude of the SH1 spurious mode in Fig. 11(c) is high. The SH1 mode can be suppressed by reducing the thickness of $LiNbO_3$ (i.e., h_{LN}/λ), but this will result in higher IL at the upper side of passband. Thus, one future work is to explore the potential of the LL-SAW devices on $LiNbO_3/SiO_2$/SiC substrate. On the other hand, a better IDT design is needed to simultaneously achieve high Q and in-band spurious-free response.

IV. CONCLUSION

In summary, high-performance LL-SAW devices based on X-cut $LiNbO_3$/SiC have been demonstrated in this article. The designed structure of the LL-SAW resonator has been optimized by the simulation to simultaneously achieve the high k_t^2, the low attenuation, and the weak spurious modes. In particular, a novel NSR structure has been applied to eliminate the lateral overtone mode in LL-SAW resonators. The fabricated resonators show high resonant frequencies from 3.75 to 4.95 GHz, large AR between 56.0 and 64.1 dB, and large k_t^2 between 18.3% and 20%. The extracted TCF at 4.19 GHz is -35.15 ppm/°C. The fabricated LL-SAW filter centered at 4.84 GHz shows a low minimum IL of 0.88 dB and a 3-dB BW of 457 MHz, partially covering the N79 band. These results show the great potential of LL-SAW technology based on the X-cut $LiNbO_3$/SiC platform to address the challenges of RF filters for 5G NR and Wi-Fi 5/6 bands.

REFERENCES

[1] A. O. Watanabe, M. Ali, S. Y. B. Sayeed, R. R. Tummala, and M. R. Pulugurtha, "A review of 5G front-end systems package integration," *IEEE Trans. Compon., Packag., Manuf. Technol.*, vol. 11, no. 1, pp. 118–133, Jan. 2021.

[2] F. Balteanu, "RF front end module architectures for 5G," in *Proc. IEEE BiCMOS Compound Semiconductor Integr. Circuits Technol. Symp. (BCICTS)*, Nov. 2019, pp. 1–8.

[3] A. Hagelauer et al., "From microwave acoustic filters to millimeter-wave operation and new applications," *IEEE J. Microw.*, vol. 3, no. 1, pp. 484–508, Jan. 2023.

[4] S. Gong, R. Lu, Y. Yang, L. Gao, and A. E. Hassanien, "Microwave acoustic devices: Recent advances and outlook," *IEEE J. Microw.*, vol. 1, no. 2, pp. 601–609, Apr. 2021.

[5] C. C. W. Ruppel, "Acoustic wave filter technology—A review," *IEEE Trans. Ultrason., Ferroelectr., Freq. Control*, vol. 64, no. 9, pp. 1390–1400, Sep. 2017.

[6] H. Zhou et al., "Surface wave and Lamb wave acoustic devices on heterogenous substrate for 5G front-ends," in *IEDM Tech. Dig.*, Dec. 2020, pp. 17.6.1–17.6.4.

[7] R. Aigner, G. Fattinger, M. Schaefer, K. Karnati, R. Rothemund, and F. Dumont, "BAW filters for 5G bands," in *IEDM Tech. Dig.*, Dec. 2018, pp. 14.5.1–14.5.4.

[8] S. Parkvall, E. Dahlman, A. Furuskar, and M. Frenne, "NR: The new 5G radio access technology," *IEEE Commun. Standards Mag.*, vol. 1, no. 4, pp. 24–30, Dec. 2017.

[9] *5G New Radio solutions: Revolutionary Applications Here Sooner Than You Think*, Skyworks, San Irvine, CA, USA, 2018. [Online]. Available: https://www.skyworksinc.com/-/media/skyworks/documents/products/2901-3000/5g-white-paper-part-2.pdf

[10] A. Tag et al., "Next generation of BAW: The new benchmark for RF acoustic technologies," in *Proc. IEEE Int. Ultrason. Symp. (IUS)*, Venice, Italy, Oct. 2022, pp. 1–4.

[11] T. Yokoyama, Y. Iwazaki, Y. Onda, T. Nishihara, Y. Sasajima, and M. Ueda, "Highly piezoelectric co-doped AlN thin films for wideband FBAR applications," *IEEE Trans. Ultrason., Ferroelectr., Freq. Control*, vol. 62, no. 6, pp. 1007–1015, Jun. 2015.

[12] R. Su et al., "Scaling surface acoustic wave filters on LNOI platform for 5G communication," in *IEDM Tech. Dig.*, San Francisco, CA, USA, Dec. 2022, pp. 4.2.1–4.2.4.

[13] H. Nakamura et al., "Suppression of transverse mode spurious in SAW resonators on an SiO_2/Al/$LiNbO_3$ structure for wideband CDMA applications," in *Proc. IEEE Int. Ultrason. Symp. (IUS)*, Beijing, China, Oct. 2008, pp. 594–597.

[14] R. Su et al., "Wideband surface acoustic wave filter at 3.7 GHz with spurious mode mitigation," *IEEE Trans. Microw. Theory Techn.*, vol. 71, no. 2, pp. 480–487, Feb. 2023.

[15] J. Wu et al., "Advanced surface acoustic wave resonators on $LiTaO_3/SiO_2$/sapphire substrate," *IEEE Electron Device Lett.*, vol. 43, no. 10, pp. 1748–1751, Oct. 2022.

[16] T. Kimura, K. Daimon, T. Ogami, and M. Kadota, "S_0 mode Lamb wave resonators using $LiNbO_3$ thin plate on acoustic multilayer reflector," *Jpn. J. Appl. Phys.*, vol. 52, no. 7S, Jul. 2013, Art. no. 07HD03.

[17] F. Matsukura, M. Uematsu, K. Hosaka, and S. Kakio, "Longitudinal-type leaky surface acoustic wave on $LiNbO_3$ with high-velocity thin film," *Jpn. J. Appl. Phys.*, vol. 52, no. 7S, Jul. 2013, Art. no. 07HD02.

[18] P. Zheng et al., "Ultra-low loss and high phase velocity acoustic delay lines in lithium niobate on silicon carbide platform," in *Proc. IEEE 35th Int. Conf. Micro Electro Mech. Syst. Conf. (MEMS)*, Tokyo, Japan, Jan. 2022, pp. 1030–1033.

[19] V. I. Grigorievski, "Fast leaky surface acoustic waves on lithium niobate and lithium tantalate," in *Proc. IEEE Ultrason. Symp.*, San Juan, PR, USA, Mar. 2000, pp. 259–262.

[20] T. Makkonen, V. P. Plessky, W. Steichen, and M. M. Salomaa, "Surface-acoustic-wave devices for the 2.5–5 GHz frequency range based on longitudinal leaky waves," *Appl. Phys. Lett.*, vol. 82, no. 19, pp. 3351–3353, May 2003.

[21] T. Makkonen, V. P. Plessky, W. Steichen, V. I. Grigorievski, M. Solal, and M. M. Salomaa, "Longitudinal leaky SAW resonators and filters on YZ-$LiNbO_3$," *IEEE Trans. Ultrason., Ferroelectr., Freq. Control*, vol. 53, no. 2, pp. 393–401, Feb. 2006.

[22] T. Takai et al., "Incredible high performance SAW resonator on novel multi-layerd substrate," in *Proc. IEEE Int. Ultrason. Symp. (IUS)*, Tours, France, Sep. 2016, pp. 1–4.

[23] T. Takai et al., "High-performance SAW resonator with simplified $LiTaO_3/SiO_2$ double layer structure on Si substrate," *IEEE Trans. Ultrason., Ferroelectr., Freq. Control*, vol. 66, no. 5, pp. 1006–1013, May 2019.

[24] M. Kadota, Y. Ishii, and S. Tanaka, "Surface acoustic wave resonators with hetero acoustic layer (HAL) structure using lithium tantalate and quartz," *IEEE Trans. Ultrason., Ferroelectr., Freq. Control*, vol. 68, no. 5, pp. 1955–1964, May 2021.

[25] S. Zhang et al., "Surface acoustic wave devices using lithium niobate on silicon carbide," *IEEE Trans. Microw. Theory Techn.*, vol. 68, no. 9, pp. 3653–3666, Sep. 2020.

[26] E. Butaud et al., "Smart Cut™ piezo on insulator (POI) substrates for high performances SAW components," in *Proc. IEEE Int. Ultrason. Symp. (IUS)*, Las Vegas, NV, USA, Sep. 2020, pp. 1–4.

[27] T. Kimura, M. Omura, Y. Kishimoto, and K. Hashimoto, "Comparative study of acoustic wave devices using thin piezoelectric plates in the 3–5-GHz range," *IEEE Trans. Microw. Theory Techn.*, vol. 67, no. 3, pp. 915–921, Mar. 2019.

[28] T. Kimura, Y. Kishimoto, M. Omura, and K. Hashimoto, "3.5 GHz longitudinal leaky surface acoustic wave resonator using a multilayered waveguide structure for high acoustic energy inement," *Jpn. J. Appl. Phys.*, vol. 57, no. 7S1, Jun. 2018, Art. no. 07LD15.

[29] L. Lv et al., "Wide band BAW filter based on single-crystalline $LiNbO_3$ thin film with insulating Bragg reflector," *IEEE Trans. Ultrason., Ferroelectr., Freq. Control*, vol. 69, no. 4, pp. 1535–1541, Apr. 2022.

[30] *Federal Standards Committee of the IEEE Ultrasonics and Frequency Control Society*, IEEE Standard 176-1987, IEEE Standard on Piezoelectricity, New York, NY, USA, 1987. [Online]. Available: https://ieeexplore.ieee.org/document/26560

[31] R. Lu, Y. Yang, A. E. Hassanien, and S. Gong, "Gigahertz low-loss and high power handling acoustic delay lines using thin-film lithium-niobate-on-sapphire," *IEEE Trans. Microw. Theory Techn.*, vol. 69, no. 7, pp. 3246–3254, Jul. 2021.

[32] B. A. Auld, *Acoustic Fields and Waves in Solids*. Melbourne, FL, USA: Krieger, 1990, pp. 357–382.

[33] K. Kamitani, M. Grimsditch, J. C. Nipko, C.-K. Loong, M. Okada, and I. Kimura, "The elastic constants of silicon carbide: A Brillouin-scattering study of 4H and 6H SiC single crystals," *J. Appl. Phys.*, vol. 82, no. 6, pp. 3152–3154, Sep. 1997.

[34] E. R. Dobrovinskaya, L. A. Lytvynov, and V. Pishchik, *Sapphire: Material, Manufacturing, Applications*. Berlin, Germany: Springer, 2009, pp. 55–176.

[35] R. Bechmann, "Elastic and piezoelectric constants of alpha-quartz," *Phys. Rev.*, vol. 110, no. 5, pp. 1060–1061, Jun. 1958.

[36] T. Takai et al., "I.H.P. SAW technology and its application to microacoustic components (invited)," in *Proc. IEEE Int. Ultrason. Symp. (IUS)*, Washington, DC, USA, Sep. 2017, pp. 1–8.

[37] L. Zhang et al., "Ultra-high Q of 11000 in surface acoustic wave resonators by dispersive modulation," *IEEE Electron Device Lett.*, vol. 44, no. 5, pp. 813–816, May 2023.

[38] P. Zheng et al., "Gigahertz acoustic delay lines in lithium niobate on silicon carbide with propagation-Q of 11174," *IEEE Electron Device Lett.*, vol. 44, no. 2, pp. 309–312, Feb. 2023.

[39] S. Inoue and M. Solal, "Spurious free SAW resonators on layered substrate with ultra-high Q, high coupling and small TCF," in *Proc. IEEE Int. Ultrason. Symp. (IUS)*, Oct. 2018, pp. 1–9.

[40] K. Hashimoto, M. Yamaguchi, G. Kovacs, K. C. Wagner, T. Ruile, and R. Weigel, "Effects of bulk wave radiation on IDT admittance on 42° YX-$LiTaO_3$," *IEEE Trans. Ultrason., Ferroelectr., Freq. Control*, vol. 48, no. 5, pp. 1419–1425, Sep. 2001.

[41] T. Takai et al., "High-performance SAW resonator on new multilayered substrate using $LiTaO_3$ crystal," *IEEE Trans. Ultrason., Ferroelectr., Freq. Control*, vol. 64, no. 9, pp. 1382–1389, Sep. 2017.

[42] E. Butaud et al., "Innovative smart Cut™ piezo on insulator (POI) substrates for 5G acoustic filters," in *IEDM Tech. Dig.*, San Francisco, CA, USA, Dec. 2020, pp. 34.6.1–34.6.4.

[43] Y. Yan et al., "Wafer-scale fabrication of 42° rotated Y-cut $LiTaO_3$-on-insulator (LTOI) substrate for a SAW resonator," *ACS Appl. Electron. Mater.*, vol. 1, no. 8, pp. 1660–1666, Jul. 2019.

[44] M. Solal et al., "Transverse modes suppression and loss reduction for buried electrodes SAW devices," in *Proc. IEEE Int. Ultrason. Symp.*, San Diego, CA, USA, Oct. 2010, pp. 624–628.

[45] A. Bogner et al., "Impact of high SC content on crystal morphology and RF performance of sputtered $Al_{1-x}Sc_xN$ SMR BAW," in *Proc. IEEE Int. Ultrason. Symp. (IUS)*, Oct. 2019, pp. 706–709.

[46] C. Moe et al., "Highly doped AlScN 3.5 GHz XBAW resonators with 16% k2eff for 5G RF filter applications," in *Proc. IEEE Int. Ultrason. Symp. (IUS)*, Las Vegas, NV, USA, Sep. 2020, pp. 1–4.

[47] J. D. Larson, P. D. Bradley, S. Wartenberg, and R. C. Ruby, "Modified Butterworth-Van Dyke circuit for FBAR resonators and automated measurement system," in *Proc. IEEE Ultrason. Symp.*, San Juan, PR, USA, Mar. 2000, pp. 863–868.

[48] S. Menendez, P. de Paco, R. Villarino, and J. Parron, "Closed-form expressions for the design of ladder-type FBAR filters," *IEEE Microw. Wireless Compon. Lett.*, vol. 16, no. 12, pp. 657–659, Dec. 2006.

[49] J. Verdú, I. Evdokimova, P. de Paco, T. Bauer, and K. Wagner, "Synthesis methodology for the design of acoustic wave stand-alone ladder filters, duplexers and multiplexers," in *Proc. IEEE Int. Ultrason. Symp. (IUS)*, Washington, DC, USA, Sep. 2017, pp. 1–4.

[50] P. J. Turner, "Network synthesis design of microwave acoustic wave filters," U.S. Patent 9 038 005 B2, May 19, 2015.

[51] Y. Yang, R. Lu, L. Gao, and S. Gong, "A C-band lithium niobate MEMS filter with 10% fractional bandwidth for 5G front-ends," in *Proc. IEEE Int. Ultrason. Symp. (IUS)*, Oct. 2019, pp. 1981–1984.

[52] P. J. Turner et al., "5 GHz band n79 wideband microacoustic filter using thin lithium niobate membrane," *Electron. Lett.*, vol. 55, no. 17, pp. 942–944, Aug. 2019.

[53] Y. Shen, P. Patel, R. Vetury, and J. B. Shealy, "452 MHz bandwidth, high rejection 5.6 GHz UNII XBAW coexistence filters using doped AlN-on-Silicon," in *IEDM Tech. Dig.*, San Francisco, CA, USA, Dec. 2019, pp. 17.6.1–17.6.4.

[54] H. Zhou et al., "A 6.1 GHz wideband solidly-mounted acoustic filter on heterogeneous substrate for 5G front-ends," in *Proc. IEEE 35th Int. Conf. Micro Electro Mech. Syst. Conf. (MEMS)*, Tokyo, Japan, Jan. 2022, pp. 1006–1009.

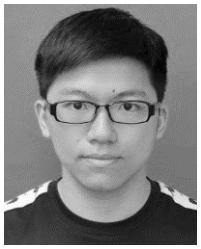

Pengcheng Zheng (Graduate Student Member, IEEE) received the B.E. degree in electronic science and technology from Southeast University, Nanjing, China, in 2019. He is currently pursuing the Ph.D. degree at the Shanghai Institute of Microsystem and Information Technology, Chinese Academy of Sciences, Beijing, China.

His current research interests include microwave filter synthesis, the design of surface acoustic wave (SAW), and lamb wave devices.

Shibin Zhang (Member, IEEE) received the B.E. degree in electronic science and technology from Southeast University, Nanjing, China, in 2015, and the Ph.D. degree from the Center of Materials Science and Optoelectronics Engineering, University of Chinese Academy of Sciences, Beijing, China, in 2020.

He was a Visiting Scholar with the Micro and Nanotechnology Laboratory, University of Illinois at Urbana–Champaign, Urbana, IL, USA. He is currently an Associate Professor with the Shanghai Institute of Microsystem and Information Technology, Chinese Academy of Sciences, Beijing. His current research interests include the design and microfabrication techniques of MEMS resonators and filters for RF front ends.

Mr. Zhang was a recipient of the 2022 IEEE Microwave Theory and Techniques (MTT) Society Microwave Prize.

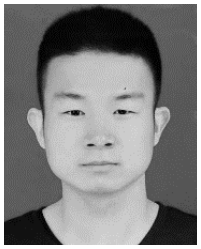

Jinbo Wu (Graduate Student Member, IEEE) received the B.S. degree in applied physics from the Hefei University of Technology, Hefei, China, in 2017. He is currently pursuing the Ph.D. degree in microelectronics and solid-state electronics with the Shanghai Institute of Microsystem and Information Technology, Chinese Academy of Sciences, Beijing, China.

His current research interests include MEMS resonators, filters, and sensors.

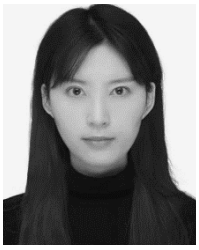

Liping Zhang (Graduate Student Member, IEEE) received the B.E. degree in inorganic nonmetallic materials engineering from the Changchun University of Science and Technology, Changchun, China, in 2018. She is currently pursuing the Ph.D. degree in microelectronics and solid-state electronics at the Chinese Academy of Sciences, Shanghai, China.

She joined the State Key Laboratory of Functional Materials for Informatics, Shanghai Institute of Microsystem and Information Technology, Chinese Academy of Sciences. Her research interests include the design and microfabrication techniques of MEMS resonators and filters for RF front ends.

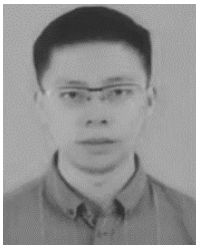

Hulin Yao (Graduate Student Member, IEEE) received the B.E. degree in applied physics from the University of Science and Technology of China, Hefei, China, in 2020. He is currently pursuing the Ph.D. degree in microelectronics and solid-state electronics with the Chinese Academy of Sciences, Shanghai, China.

He joined the State Key Laboratory of Functional Materials for Informatics, Shanghai Institute of Microsystem and Information Technology, Chinese Academy of Sciences. His research interests include the design and microfabrication techniques of MEMS resonators, filters, and integrated phononic devices.

Xiaoli Fang (Graduate Student Member, IEEE) received the B.E. degree in microelectronics science and engineering from Jiangnan University, Wuxi, China, in 2021. She is currently pursuing the Ph.D. degree with the Shanghai Institute of Microsystem and Information Technology, Chinese Academy of Sciences, Beijing, China.

Her current research interests include the simulation and design of surface acoustic wave (SAW) devices, including resonators, sensors, and filters.

Yang Chen received the B.E. degree in materials science and engineering from Southeast University, Nanjing, China, in 2018, and the Ph.D. degree in microelectronics and solid-state electronics from the University of Chinese Academy of Sciences (CAS), Beijing, China, in 2023.

He is currently the Research and Development Manager with Shanghai Novel Si Integration Technology, Shanghai, China. His current research interests include high-performance surface acoustic wave devices and integrated-optical device fabrication.

Kai Huang received the B.E. degree in microelectronics from Jilin University, Changchun, China, in 2013, and the Ph.D. degree in microelectronics and solid-state electronics from the University of Chinese Academy of Sciences (CAS), Beijing, China, in 2018.

He is currently an Assistant Researcher with the Shanghai Institute of Microsystem and Information Technology, CAS. His current research interests include the research and development and mass production of piezo thin films on heterogeneous substrates.

Xin Ou (Senior Member, IEEE) received the Ph.D. degree in microelectronics and solid-state electronics from the Shanghai Institute of Microsystem and Information Technology (SIMIT), Chinese Academy of Sciences, Shanghai, China, in 2010.

He is currently a Professor with the State Key Laboratory of Functional Material for Informatics, SIMIT. He has authored more than 80 SCI papers and has been authorized 14 patents. His current research interests include the heterointegration of functional materials for high-performance electrical, optical, and acoustical devices, especially the piezoelectric hybrid substrate for 5G RF-filter application.

Dr. Ou was a recipient of the "IBMM Prize" of the 20th International Conference on Ion Beam Modification of Materials, the "Young Investigator Award" of the 18th International Conference on Ion Implantation Technology (IIT 2010), the "Research Prize" of Helmholtz Zentrum Dresden Rossendorf Germany, the Beijing "Science and Technology Progress Award" (first grade), the "2019 Ten Achievements of Optics" in China, and the "Excellent Doctor Degree Dissertation Award" of the Chinese Academy of Sciences.